Proceedings of the ASME 2020
14th International Conference on Energy Sustainability
ES2020
June 7-11, 2020, Denver, CO, USA

SAND2019-15214C

ES2020-9783

EVALUATION OF PERFORMANCE FACTORS FOR A MULTISTAGE FALLING PARTICLE RECIEVER

Reid Shaeffer, Brantley Mills, Lindsey Yue, and Clifford K. Ho
Sandia National Laboratories
Albuquerque, New Mexico, 87185-1127, USA
rshaeff@sandia.gov

ABSTRACT

An important factor identified for the efficiency of falling particle concentrating solar applications is the falling particle curtain opacity. Low curtain opacity results in increased radiative losses. Candidate multi-stage configurations that can increase particle-curtain opacity were simulated for the existing 1 MW_{th} falling particle on-sun receiver at Sandia's NSTTF. In the candidate configurations, falling particles were collected periodically in sloped troughs spanning the width of the receiver. A small lip at the front of each trough causes particles to accumulate, allowing subsequent particles to spill over. Particle surface boundary conditions were represented with an empirically based model created to approximate particle behavior observed in testing. Curtain opacity increased using a multi-stage approach and decreases in radiative losses were outweighed by decreases in advective losses which were the dominant loss mechanism. The ability to alter the flow of air within the receiver using multi-stage release resulted in the greatest efficiency gains by reducing advective losses. Additionally, multi-stage release substantially decreased back wall temperatures within receiver.

Keywords: concentrating solar power, falling particle, receiver, thermal efficiency, multi-stage.

1. INTRODUCTION

The thermal efficiency of falling particle receivers for concentrating solar applications is dependent upon how solar irradiation is absorbed by the particles. A more opaque falling particle curtain will result in higher thermal efficiencies [1]. However, particle curtains in freefall suffer from decreased opacity with increasing fall distance. Decreased curtain opacity results in lower solar energy collection caused by increased radiative losses. Depending on construction and solar concentration, heating of receiver interior surfaces from decreased curtain opacity may result in temperatures exceeding material limits.

Several solutions have been investigated to address curtain opacity. Ho et al. [1] examined how the curtain shape may be altered to offer better performance. Increasing the curtain's depth by releasing particles with a tortuous cross section increased receiver efficiency. An emerging alternative method of maximizing particle curtain densities and opacities during freefall is to periodically collect and release particles. This approach of controlling particle descent, frequently referred to as a multi-stage approach, has appeared recently in the literature using different techniques. Ho et al. first tested a method of obstructing particle flow by releasing particles onto an array of staggered chevron features. The chevron structures reduced the particle terminal velocity by an order of magnitude compared to freefall [2, 3, 4]. The 316 stainless steel mesh chevrons were found to degrade under high temperature usage.

Experimental measurements were taken to understand the correlation between curtain volume fraction and opacity, showing that curtain volume fraction quickly decreases from 60% at the release point to less than 10% within 0.5 m from release [3]. These conclusions were confirmed numerically by Kumar et al. [5]. Arising from these studies, the multi-stage concepts investigated here were proposed by Australia's Commonwealth Scientific and Industrial Research Organization (CSIRO) and Sandia National Laboratories [6, 7]. In the candidate NSTTF on-sun configuration, falling particles are collected periodically in sloped troughs spanning the width of the receiver. A small lip at the front of each trough causes particles to accumulate, allowing subsequent particles to spill over. This behavior was captured by Yue et al. during cold flow testing at the NSTTF [8]. Ho et al. previously used the same particles when investigating different release patterns to increase efficiency and for characterizing the optical and ballistic properties of a freefalling curtain [1, 3]. Yue et al. conducted cold flow experiments with different trough angles, spacings, and mass flow rates. The behaviors observed motivated the approach

Sandia National Laboratories is a multimission laboratory managed and operated by National Technology & Engineering Solutions of Sandia, LLC, a wholly owned subsidiary of Honeywell International Inc., for the U.S. Department of Energy's National Nuclear Security Administration under contract DE-NA0003525.

described here to model particles with multi-stage release. Methods used to analyze multi-stage release for falling particle receivers in ANSYS Fluent will be discussed, along with performance factors influenced by multi-stage release. Lastly, a summary will be presented with suggestions to further increase receiver efficiency.

2. COMPUTATIONAL MODEL

A model of the existing on-sun receiver at the NSTTF was developed using ANSYS Fluent 19.4. Although the receiver is housed within a larger structure, only the receiver geometry was modeled. The unrepresented structure geometry is not expected to significantly alter the results of modeling the receiver alone in quiescent conditions. The analysis was conducted using a coupled Eulerian-Lagrangian CFD model. The computational domain included the receiver solid geometry within a 10 m x 14 m fluid region, the shorter distance referring to height parallel with gravity. The large size of the fluid region was chosen to remove fluid domain edge effects. The receiver was roughly centered within the domain extents as shown in Figure 1. Meshing was carried out in a manner comparable to that examined by Mills et al. [9] to ensure adequate discretization of the problem.

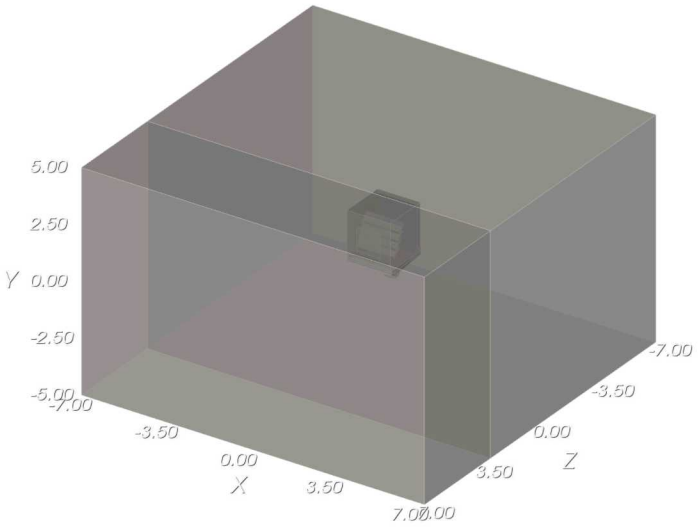

Figure 1. NSTTF on-sun receiver geometry modeled within a 10 m x 14 m fluid domain. The internal plane at z = 3.0 m was used to apply the discrete ordinates beam boundary condition.

2.1 Model Description

The interior temperatures of the receiver are substantially higher than the surrounding ambient air during operation. This causes regions of the model to achieve substantial Grashof numbers and consequentially important natural convection modes of heat transfer. Traditionally a Boussinesq approximation may be applied to couple energy and momentum equations. However, the accuracy of the Boussinesq approximation decreases with large temperature changes due to the assumption that density varies linearly with temperature. The difference in air temperatures in the NSTTF receiver may be 500-900°C relative to ambient air temperature. For such a large temperature range empirical air densities were described in terms of temperature using a piecewise linear equation rather than a Boussinesq approximation. Additionally, accounting for advective losses out of the receiver driven by buoyancy required two-way coupling with solid as well as particle regions.

Particle regions were tracked in a Lagrangian fashion. Previous studies have shown that particle curtain mass fractions near test conditions in the NSTTF decrease below 10% shortly after release [3]. An Eulerian-Lagrangian approach is more appropriate than an Eulerian-Eulerian representation for this regime of particle mass fraction where behavior is dominated by fluid-particle interactions rather than particle-particle collisions. Curtain opacity is defined as the ratio of light intercepted by the curtain to the total amount of light incident upon the curtain [3]. Curtain opacity is not readily calculated in simulation for Lagrangian particles. However, a proportional metric of volume fraction is available and has been used to relate radiative losses [10].

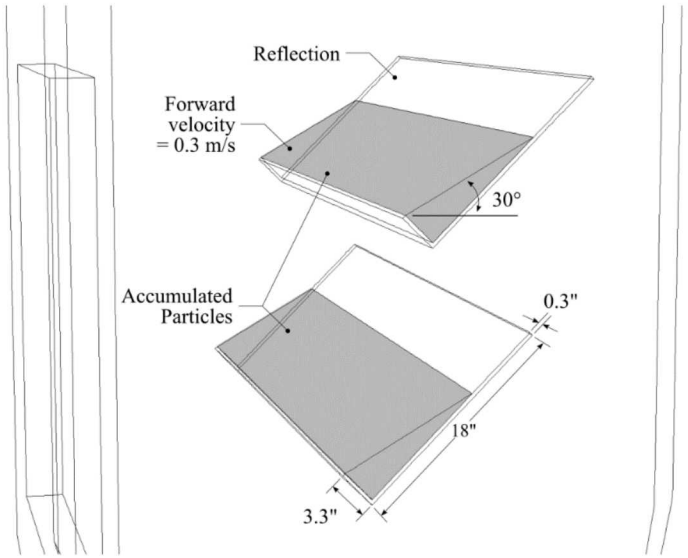

Figure 2. Detail view of how particle boundary conditions were applied on trough surfaces.

Radiation within the model was solved using a discrete ordinates method. Irradiance from the NSTTF heliostat field was applied as a discrete ordinates beam profile. The beam was prescribed on the internal surface at z = 3.0 m in Figure 1. Using NREL's ray tracing code SolTrace, the beam intensity and directionality from the NSTTF heliostat field was computed for a surface located 3.0 m from the aperture. The radiation model included a grey, banded wavelength approximation. Irradiation from the sun corresponded to smaller wavelengths in the band from 0.1-2.5 μm, while thermal radiation occurred in bands of 2.5-4.5 μm and 4.5-100 μm. Assuming the sun behaves as a blackbody, Planck's law defines that 96% of solar irradiation is concentrated in the wavelength band of 0.1-2.5 μm. The distinction between longer wavelength bands was set according to the emissive properties of the silica refractory panels lining the NSTTF on-sun receiver. The refractory panels have a low emissivity in the first and second band, with most emission

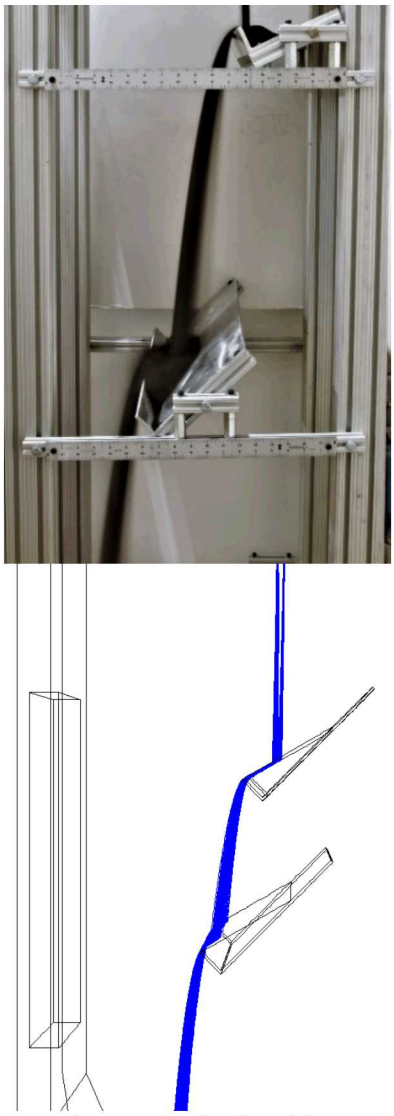

Figure 3. Experimental versus simulated particle curtain behavior in multi-stage troughs. Left photo by Yue et al., particle mass flow rate of 0.62 kgs^{-1} [8].

occurring in the longest wavelength band [1]. This division according to wavelength leads to two valuable categories of radiation from the receiver, reflected and thermal radiation.

2.2 Particle Surface Interactions

Yue et al. and Kim et al. [8, 6] experimentally tested multi-stage release using similar troughs to those simulated here. The photograph taken by Yue et al. shown in Figure 3 motived the particle modeling approach described here. The steel multi-stage troughs were modeled as solid volumes as shown in Figure 2. During cold flow testing, it has been observed that particles will accumulate in the trough with a free surface angle corresponding approximately to the angle of repose. The angle of repose for the CARBO HSP particles has been measured to be approximately 30°. The portion of the trough not covered by accumulated particles remains bare metal. Particles that impact the free metal trough surface reflect with nearly elastic collisions given the hardness of the alumina CARBO HSP particles used in testing [11]. Particle to bare metal collisions are undesirable in operation as it leads to ejection of particles out of the receiver and particle dispersion. Simulated Lagrangian particles that impacted the surface of solids representing accumulation react according to a user-defined function. Particles impacting aggregate accumulations will experience dampening as a portion of the kinetic energy displaces other accumulated particles. This behavior is also observed during cold particle flow testing as shown in Figure 3. To mimic this behavior, particles that impact surfaces representing accumulation are assigned a small forward velocity of 0.3 ms^{-1}, while velocity is eliminated for all other directions. The small forward velocity value was chosen to approximate the behavior observed in cold flow testing.

Alternatively, a low coefficient of restitution could be applied for particle-to-accumulation collisions. However, numerical issues arise when using a low coefficient of restitution for Lagrangian particles. The coefficient of restitution required to approximate observed particle behavior is quite low. Particles lose substantial momentum with each successive impact with accumulation surfaces. For particles that impact the surface more than once, velocity is quickly deceased to very small values such that particles are trapped.

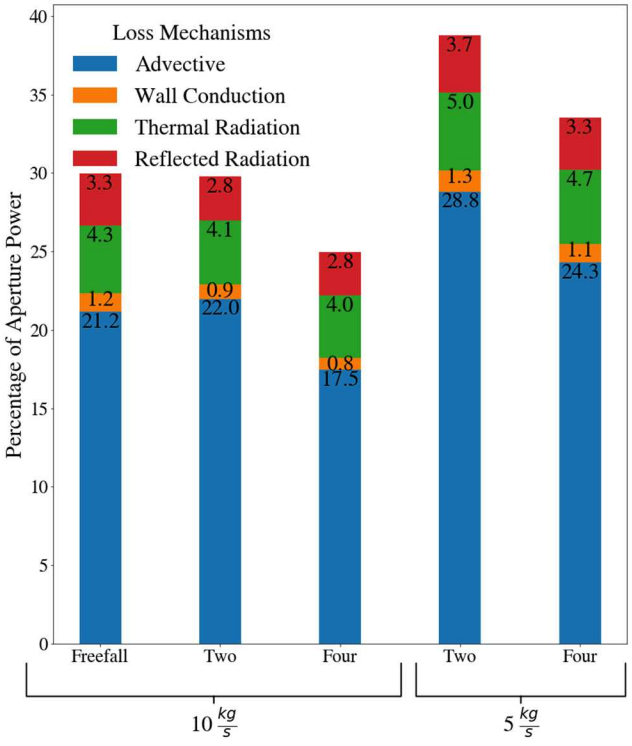

Figure 4. Losses mechanisms for various multi-stage configurations. Losses are represented as a percentage of power from the heliostat field.

Approximating particles impacting the surface of accumulations with a low coefficient of restitution would be feasible for the first interaction, however subsequent interactions would not account for rolling or sliding of the particle across the surface. An option for future simulations may be to create a hybrid boundary condition with a coefficient of restitution and a velocity threshold. Particles that reflect with a velocity magnitude below a threshold value would be treated as elastic collisions to prevent exponentially decaying velocities.

2.3 Radiative Losses

Various configurations for a multi-stage receiver were simulated for the NSTTF on-sun receiver. These cases include no multi-stage release, 2 stages, and 4 stages. The boundary conditions were identical for all 5 cases and are summarized in Figure 4.

Most notably, the radiative losses out of the receiver did not substantially change with the addition of multi-stage releases. Although average curtain volume fraction increased resulting in increased opacity as shown in Figure 6, radiative losses did not decrease accordingly. This behavior may be attributed to the receiver's cavity geometry and construction.

Consider the adiabatic cavity of arbitrary shape with only one opening over which a hypothetical window with a transmissivity τ of unity in all wavelengths is placed to eliminate advective losses as shown in Figure 5. Allow a curtain of blackbody particles to fall inside of the cavity, just behind the window. All radiation incident upon the window will either be absorbed by the curtain or enter the cavity. Under steady state conditions, energy entering the cavity not absorbed by the curtain must be directed outward due the perfect insulation of the cavity. Therefore, radiation that is reflected out of the cavity must pass through the curtain a second time without being absorbed. The probability for radiation to pass through a sufficiently opaque particle curtain twice is not substantially altered by increasing the curtain opacity further. This analogy requires that the curtain completely obstruct the receiver aperture such that no radiation from the cavity may be emitted without passing through the curtain. For the NSTTF on-sun receiver, the curtain nearly spans the width of the receiver interior to obstruct the surfaces behind it. The curtain in the NSTTF on-sun receiver is 1.12 m wide, while the interior of the receiver is 1.57 m wide.

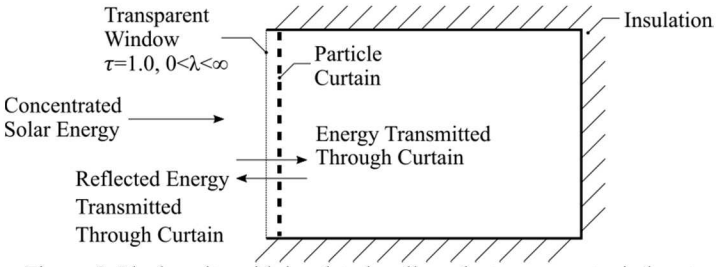

Figure 5. Ideal cavity with insulated walls and a transparent window to eliminate advective losses.

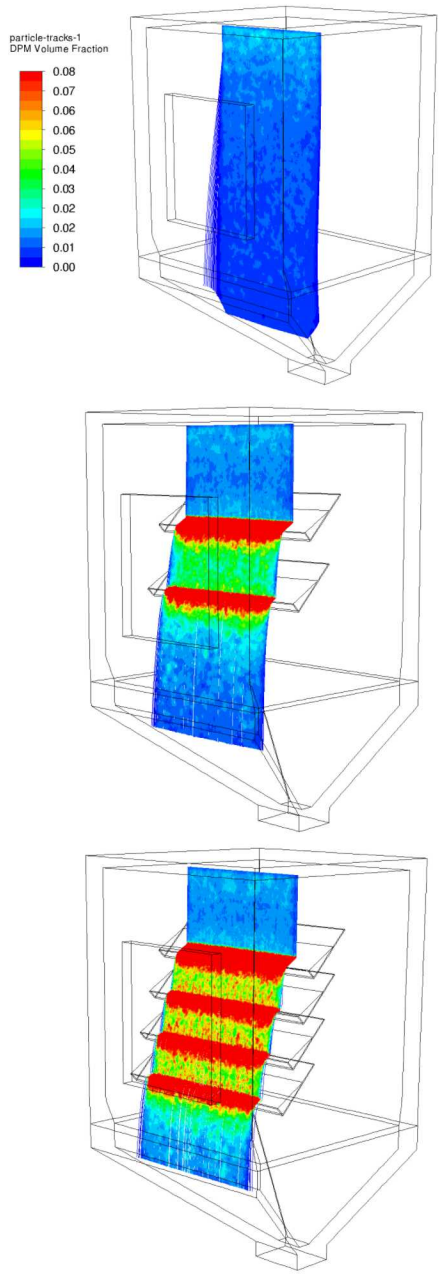

Figure 6. Particle volume fraction at a particle mass flow rate of 10 kgs-1 (a) without troughs (b) with 2, and (c) with 4 troughs. Trough collection areas have mass fractions higher than 8%, the color bar scale causes clipping in these areas.

A second assumption is that the walls of the cavity are perfectly insulated. For the NSTTF on-sun receiver, conduction losses through the receiver walls represent a fraction of <1.5% of the energy entering the aperture. The NSTTF on-sun receiver walls were heavily insulated to minimize conduction losses.

2.4 Interior Wall Temperatures

In practice, the silica refractory panels lining the NSTTF on-sun receiver have an upper temperature limit of approximately 1760°C [1], although temperatures above 1000°C are avoided during extended testing. Radiation that initially passes through the curtain irradiates the interior of the receiver potentially leading to temperatures exceeding material limits. For the case without multiple stages, the simulated peak back wall temperature was approximately 996°C. The addition of multi-stage troughs reduced this value to 912°C and 793°C for 2 and 4 troughs, respectively as shown in Figure 7.

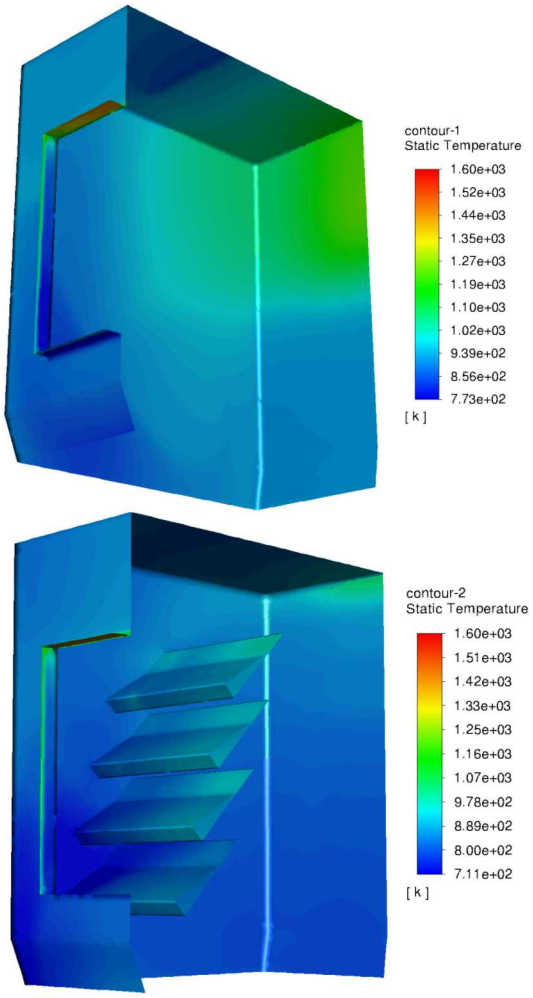

Figure 7. Peak back wall temperatures without and with 4 multi-stage troughs for cases with a particle mass flow rate of 10 kgs^{-1}.

Although radiative losses did not change substantially, advective losses were decreased by a significant amount. Examining the velocity vectors for a slice of the domain taken at the east/west mid-plane of the receiver, a change in behavior near the lower aperture edge may be seen in Figure 8. The particle curtain was translated closer to the lower edge of the aperture when 4 troughs were included. Minimizing the distance between the curtain and lower aperture edge created more resistance to ambient air entering the receiver. Cool, ambient air that enters the receiver adversely convects heat from the particle curtain. Minimizing the ability of external ambient air to enter the receiver minimized advective losses for increased receiver efficiency. Translating the particle curtain to the aperture must be balanced with minimizing particle loss.

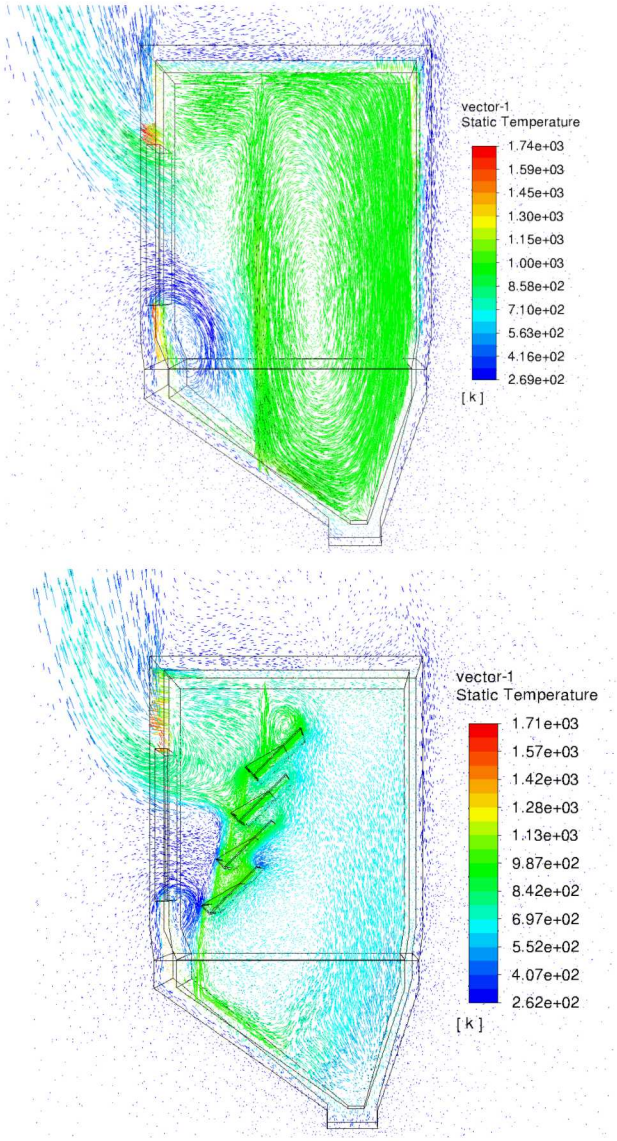

Figure 8. Velocity vector plots taken at the receiver mid-plane for cases with a particle mass flow rate of 10 kgs^{-1}. Vectors are colored by the air temperature.

3. CONCLUSIONS

The existing NSTTF on-sun receiver was analyzed with the inclusion of multi-stage release using ANSYS Fluent. Loss mechanisms for simulations without, with 2, and with 4 multi-stage troughs were compared to understand how multi-stage release affects receiver efficiency. Although the addition of

multi-stage increased curtain particle volume fractions, radiative losses out of the receiver were not reduced significantly. Receiver designs with longer particle freefall lengths and resulting decreases in curtain opacity will benefit from multi-stage release through larger reductions in radiative losses. Radiative losses were already small in the NSTTF on-sun receiver design thus limiting the gains from improved curtain opacity. Alternatively, the addition of multi-stage troughs altered the airflow within the receiver to minimize ingress of cool ambient air. Although radiative losses were not significantly decreased, multi-stage release also does offer decreased back wall temperatures enabling a wider range of operating conditions.

ACKNOWLEDGEMENTS

This work was funded by the DOE Solar Energy Technologies Office and Gen 3 CSP program. Sandia National Laboratories is a multi-mission laboratory managed and operated by National Technology and Engineering Solutions of Sandia, LLC., a wholly owned subsidiary of Honeywell International, Inc., for the U.S. Department of Energy's National Nuclear Security Administration under contract DE-NA0003525.

REFERENCES

[1] C. K. Ho, B. Mills and J. M. Christian, "Volumetric Particle Receivers for Increased Light Trapping and Heating," in *Proceedings of the ASME 2016 10th International Conference on Energy Sustainability*, 2016. https://doi.org/10.1115/ES2016-59544.

[2] C. K. Ho, J. M. Christian, J. E. Yellowhair, K. Armijo, W. J. Kolb, S. Jeter, M. Golob and C. Nguyen, "On-Sun Performance Evaluation of Alternative High-Temperature Falling Particle Receiver Designs," *J. Sol. Energy Eng.,* 2019. https://doi.org/10.1115/1.4041100.

[3] C. K. Ho, J. M. Christian, D. Romano, J. Yellowhair, N. Siegel, L. Savoldi and R. Zanino, "Characterization of Particle Flow in a Free-Falling Solar Particle Receiver," in *Journal of Solar Energy Engineering*, ASME, 2017. https://doi.org/10.1115/1.4035258.

[4] C. K. Ho, J. M. Christian, J. Yellowhair, N. Siegel, S. Jeter, M. Golob, S. I. Abdel-Khalik, C. Nguyen and H. Al-Ansary, "On-Sun Testing of an Advanced Falling Particle Receiver System," in *AIP Conference Proceedings*, 2015.

[5] A. Kumar, J.-S. Kim and W. Lipinski, "Radiation Absorption in a Particle Curtain Exposed to Direct High-Flux Solar Irradiation," *Journal of Solar Engineering,* vol. 140, 2018.

[6] J.-S. Kim, A. Kumar, W. Gardner and W. Lipinski, "Numerical and Experimental Investigation of a Novel Multi-Stage Falling Particle Receiver," in *SolarPACES*, 2018.

[7] A. Kumar, W. Lipin´ski and J.-S. Kim, "Numerical modelling of radiation absorption in a novel multi-stage free-falling particle receiver," *International Journal of Heat and Mass Transfer,* vol. 146, 2019. https://doi.org/10.1016/j.ijheatmasstransfer.2019.118821.

[8] L. Yue, "PAPER TITLE".

[9] B. Mills and C. K. Ho, "Simulation and performance evaluation of on-sun particle receiver tests," in *AIP Conference Proceedings*, 2019. https://doi.org/10.1063/1.5117548.

[10] F. Ordonez, C. Caliot, F. Bataille and G. Lauriat, "Optimization of the optical particle properties for a high temperature solar particle receiver," *Solar Energy,* vol. 99, pp. 299-311, 2014.

[11] K. Kim, S. F. Moujaes and G. J. Kolb, "Experimental and simulation study on wind affecting particle flow in a solar receiver," *Solar Energy,* vol. 84, pp. 263-270, 2010.